A 23 μA RF-Powered Transmitter for Biomedical Applications

Fan Zhang, Matthew A. Stoneback, and Brian P. Otis

Department of Electrical Engineering, University of Washington, Seattle, WA 98195-2500

***Abstract*—We propose a new tag architecture that employs an active transmitter to decouple the frequencies used for power and data telemetry. Receiving power at 918 MHz and transmitting data at 306 MHz eliminates the "self-jamming" problem presented to RFID readers, reducing the complexity of reader design. This scheme allows remote placement of the data receiver and extends the data transmission range. Our transmitter uses subharmonic injection-locking to avoid power hungry LO generation circuitry while eliminating the need for quartz crystals. The tag prototype was fabricated using a 0.13 μm CMOS process, occupying 0.3 mm^2 active area. With an on-off keying (OOK) data rate of 4 Mbps, the 23 μA transmitter with an output power of -33 dBm achieves an energy efficiency of 10 pJ/bit, the best reported to date for such systems.**

***Index Terms*—Biomedical telemetry, radio transmitters, RFID tags, low-power electronics, body sensor networks, injection-locked oscillators, amplitude modulation, amplitude shift keying, ring oscillators**

I. Introduction

Recently, there has been a growing demand for the integration of sensing and telemetry in diverse applications, including biosignal monitoring and smart buildings. For unobtrusive body-worn applications, both wireless data and power transmission are necessary because real-time biomedical data is otherwise inaccessible, and replacing batteries is undesirable.

Several power supply solutions have been proposed, including using a battery or an inductive link. Unfortunately, battery-powered sensors suffer from limited lifespan while inductive-coupling suffers from short (on the order of cm) wireless ranges. Others have used passive radio frequency identification (RFID) technologies to reduce the power consumption of the data transmission circuitry, thus extending the range of wireless power transfer [1][2]. However, the reader design is complex, partially because it must detect faint backscattered signals at the same frequency power is transmitted. Many commercial readers implement the Gen2 RFID protocol, which leads to a significant increase in tag complexity and transmit overhead. We introduce a passive tag architecture that decouples the power and data transmission, thus reducing the complexity of the reader.

Fig. 1 illustrates the proposed system architecture. The proposed tag architecture has the same wireless power transfer scheme as RFID systems, but actively transmits at 1/3 of the input frequency to avoid the "self-jamming" problem presented to conventional RFID readers. We use subharmonic injection-locking to avoid complex LO-generation circuitry while eliminating the need for quartz crystals. Though the downlink range (power delivery) is comparable to existing RFID systems, we demonstrate a far greater uplink range (sensor data transmission), thus improving receiver mobility.

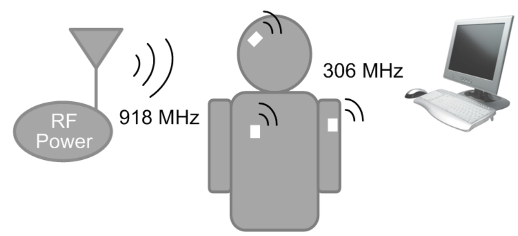

Fig. 1. High-level system architecture. Passive tags are remotely powered and perform sensing. Data is transmitted at a 1/3 frequency carrier derived from the RF power through injection locking.

II. Literature Overview

Existing active transmitter topologies operating at low carrier frequencies (<100 MHz) typically consume less power and experience less tissue absorption than those operating at high frequencies [3]. However, in applications where small antenna sizes, high data rates (on the order of a few hundred kbps), and longer range are required, it is desirable to operate at higher frequencies (> 100 MHz). To avoid RF heating of the tissue, the FCC has mandated maximum permissible exposure (MPE) levels, which are especially stringent at high frequencies due to increased tissue absorption. It is therefore critical to reduce the power consumption of the tag, particularly in the active transmitter. Published implantable transceiver designs usually operate LC or ring oscillators in open loop [4][5]. LC oscillators consume relatively high power especially when low-Q on-chip inductors are employed. Ring oscillators consume less power, but are plagued with high phase noise and poor frequency stability.

In [6], the input RF signal powers the chip and injection-locks a frequency-doubling LC oscillator to generate an accurate system clock. The LC oscillator and choice of transmit frequency resulted in a high current consumption of 2 mA. Therefore, the system needs be heavily duty-cycled, precluding its use in continuous streaming applications.

III. Proposed Architecture and Circuit Design

Fig. 2 illustrates the proposed system block diagram. By transmitting in a different band than the RF power source, a conventional ASK narrowband receiver can be used instead of a complex RFID reader. Without having to comply with RFID protocols, the complexity of the proposed tag and the transmit overhead can also be reduced. The downlink (918 MHz) and uplink (306 MHz) frequencies are harmonically related and

978-1-4244-8292-4/11/$26.00

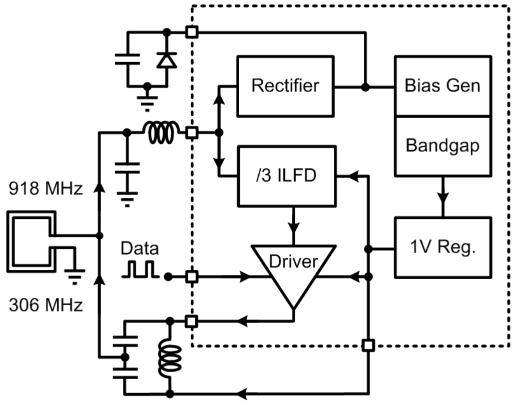

Fig. 2. Block diagram of the proposed transmitter tag architecture.

were chosen to fall into established frequency bands with sufficiently high radiated power permitted by FCC.

We designed a dual-band antenna to allow simultaneous uplink and downlink transmission. After impedance-transformation by an L-match network, the incident RF signal splits into two paths. In one path, the input voltage is rectified and subsequently regulated to 1 V. The energy is stored in an off-chip 10 μF capacitor. In the other path, the input RF signal injection-locks a subharmonic ring oscillator, performing divide-by-3 functionality. The divider output is then AC-coupled to an open-drain driver. Binary data is OOK-modulated by power-cycling the driver. We chose OOK modulation here to conserve power during transmission of the "1" symbols. The driver's load impedance is transformed through a tapped capacitor network to match to the 50 Ω antenna. Using this scheme, a stable low power high-frequency reference is obtained.

A. Injection-locked Frequency Divider (ILFD)

Injection-locked frequency dividers (ILFDs) usually consume less power than conventional flip-flop-based dividers. Compared to injection-locked LC-based dividers, ring-oscillator (RO) ILFDs offer smaller areas and larger locking range. The notoriously poor phase noise of ring oscillators is also improved dramatically in the injection locking process.

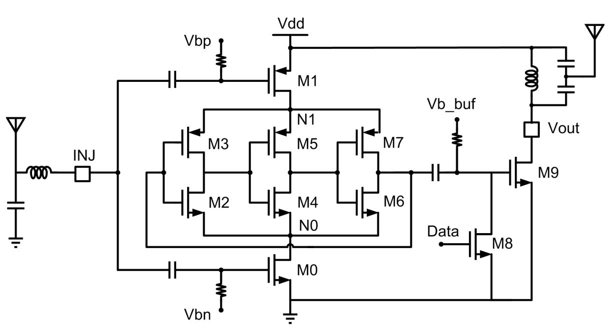

Fig. 3. Schematic of the injection-locked divide-by-3 circuit.

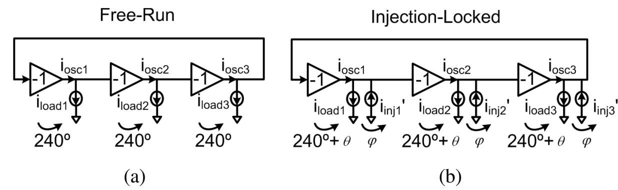

Fig. 4. Phase relationship between the current and voltage components and small-signal equivalent circuit of the ILFD when in a a) free running and b) injection-locked condition.

Fig. 3 shows the schematic of the proposed 3-stage ILFD. Separation of the signal and bias paths through AC-coupling allows the input to simultaneously inject into M_0 and M_1, producing injection currents i_{inj} at the $N_{0,1}$. The transistors M_{2-7} function as sub-harmonic mixers that translate the harmonics of i_{inj} and i_{osc} into the sum and difference frequency components $|m \cdot f_{inj} \pm n \cdot f_{osc}|$ at the inverter outputs. When injecting a sufficiently strong signal within the locking range of the ILFD, the ring oscillator will lock to the frequency component closest to its f_o (1/3$\cdot f_{inj}$ here).

Fig. 4 graphically depicts the injection-locking process. When the oscillator free-runs, the three identical stages equally distribute $180° + n \cdot 360°$ phase shift around the loop, and each stage has a phase shift of $240°$. Injection of $i_{inj'}$ ($= K \cdot i_{inj}$, K being the mixer conversion gain) shifts i_{load} by ϕ. The circuit is forced to oscillate at a different frequency such that each stage will contribute additional delay θ to cancel ϕ and the total phase shift around the loop remains $180° + n \cdot 360°$.

The locking range is directly proportional to $\frac{|i_{inj}|}{|i_{osc}|}$. Injecting complementary signals into the top and bottom tails of multiple inverter stages doubles the injection strength, thus widening the locking range. In addition, the complementary injection drives both the rising and falling propagation delays, compared to the conventional tail-injection schemes where either rising or falling propagation delay are varied [7]. Consequently, the oscillation frequency and duty cycle can be better controlled.

In the proposed architecture, the power of the incident RF signal that injection-locks the ILFD and powers the chip is not well-controlled. Locking under high input power conditions is limited by the undesired non-linearity of the ILFD. To mitigate this locking deficiency at high input power, the tail transistors use low-V_t devices with small aspect ratios to improve device linearity. This phenomenon could also be prevented by limiting the input power injected into the ILFD.

B. Power Management

The RF rectifier uses a 6-stage voltage-doubling charge-pump topology [1]. We chose zero-V_t devices with low forward voltage drop and tolerable back-leakage to provide good sensitivity and efficiency. The output is clamped at 3 V with an off-chip Zener diode for over-voltage protection.

Bias currents for the chip are generated by a V_{gs}/R reference that maintains a stable output current of 45 nA from 0.6 V to 3.6 V [1]. A bandgap reference provides a temperature-independent reference voltage that is stable to within 4 mV (of

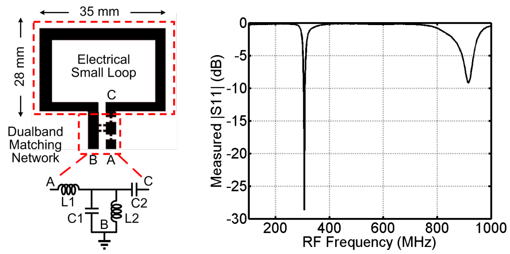

(a) (b)

Fig. 5. a) CAD drawing of the custom loop antenna and its dual-band matching network; b) Measured antenna input return loss.

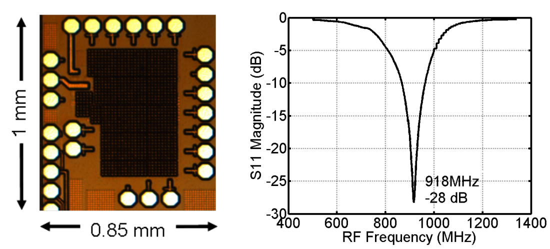

(a) (b)

Fig. 6. a) The chip micrograph of the transmitter tag; b) Measured input return loss.

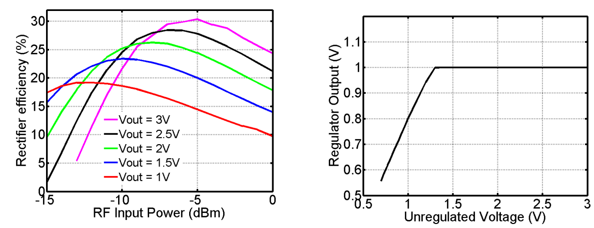

(a) (b)

Fig. 7. a) Measured rectifier efficiency vs. input power; b) Measured regulator output voltage vs. input voltage.

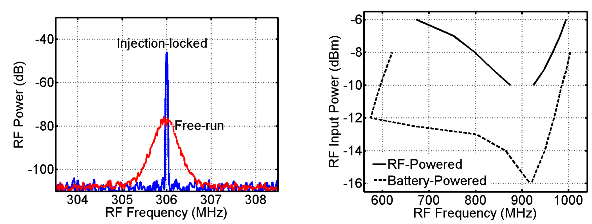

(a) (b)

Fig. 8. a) Spectrum of the free-running and injection-locked ILFD; b) Measured injection locking range.

the nominal 1.2 V) across 0-100°C. A low-drop-out (LDO) linear regulator provides stable 1 V supply for the ILFD and driver.

C. Antenna Design

The loop antenna is sized such that the circumference of the loop is $\sim \lambda/4$ at a frequency that lies between the input (918MHz) and output frequency (306MHz). The reactance looking into the loop antenna is inductive at 918 MHz and capacitive at 306 MHz. Since the input impedance at both frequencies is low, a dual-band matching network is used to provide relatively independent control of impedance matching at both frequencies. A drawing of the small loop antenna with dual band UHF matching network is shown in Fig. 5(a). L_1 and C_1 are used to match to 918 MHz, while L_2 and C_2 are used to match to 306 MHz. The fabricated antenna is populated with surface mount components that comprise the matching network. The return loss response of the assembled antenna was measured using an Agilent 8720 VNA as shown in Fig. 5(b).

IV. Measurement Results

The 918MHz/306MHz tag prototype was fabricated in a 0.13 μm CMOS process. The total current consumption of the chip varies from 19 to 23 μA as the input power increases from -10 to -6 dBm. The die photo is shown in Fig. 6(a). The total active area is 450 $\times$ 650 μm^2. Fig. 6(b) shows the measured input return loss $|s_{11}| <$ -28 dB for downlink port.

Fig. 7(a) shows the measured rectifier efficiency as a function of input power. The efficiency is 20-30% for typical RF input power at output $>$ 1 V. Fig. 7(b) shows the regulator output voltage as a function of input unregulated voltage. The minimum unregulated voltage required for regulation (dropout voltage) is 1.3 V.

Fig. 8(a) shows the overlaid spectrum of free-running and injection-locked ILFD. The output power when injection-locked is higher due to the increase in the output swing. The close-in phase noise of the ILFD inherits the phase noise of the RF power source when injection-locked. The measured input power range as a function of operating frequency for locking is shown in Fig. 8(b). The measured maximum locking range is 51% (575 MHz to 969 MHz) when powered with a battery (dashed) and 39% (673 to 995 MHz) when RF-powered (solid), ensuring injection-locking across realistic PVT variations. In the latter case, the range of input power for locking is limited on the low side by the minimum power required to supply to the circuitry and on the high side by the maximum power before the ILDF non-linearity prevent proper injection-locking.

OOK data modulation is verified by externally supplying a digital modulation signal. Fig. 9(a) shows the transmitter output spectrum corresponding to the driver power-cycled at 2 MHz (4 Mbps data rate). Fig. 9(b) shows the transient output waveform when OOK-modulated by a 2 MHz square-wave. The high on/off contrast ratio in the modulated output relaxes the requirements on the OOK receiver. A start-up time of $<$ 100 ns is achieved, allowing aggressive transmitter duty-cycling.

Fig. 10(a) shows the experimental setup that verifies the functionality of the wireless power and data transmission links. This experiment was performed in a laboratory environment.

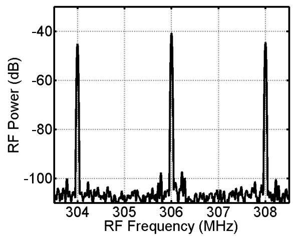

(a)

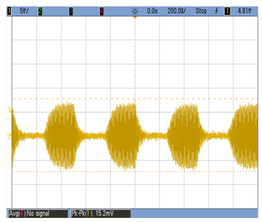

(b)

Fig. 9. a) Spectrum b) transient waveform of OOK-modulation at 4 Mbps.

Complying with the FCC regulation, an Agilent E8254A signal generator transmitted a +35 dBm EIRP continuous wave at 918 MHz to the chip through a horn antenna. The input and output of chip are both connected to the custom loop antenna. An MSP430 microcontroller supplied the data stream to the chip. The loop antenna simultaneously receives power at 918 MHz from the horn antenna located 1.3 m away and transmits the 306 MHz OOK signal to a commercial Melexis TH7122 receiver. Fig. 10(b) shows the binary data (top) from the MSP430 and the data faithfully demodulated by the receiver located 6 meters away (bottom). The 20 kpbs data rate chosen here is limited by the maximum OOK data rate of the receiver.

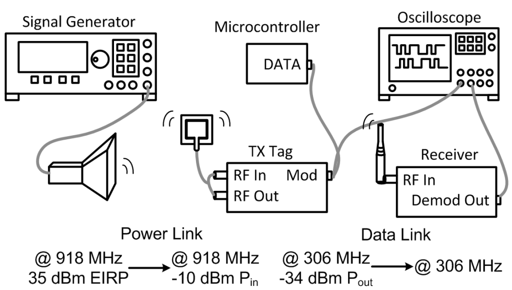

(a)

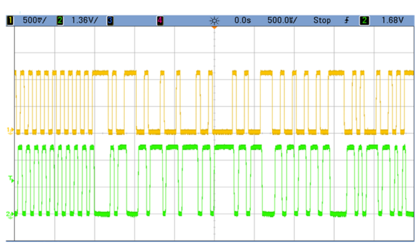

(b)

Fig. 10. a) Wireless link test setup; b) Baseband OOK-modulation signal and received/demodulated signal at 20 kbps.

Table I summarizes the performance of the proposed chip with a few recently published transmitters used in biomedical systems. The P_{out} is measured at the distance reported. At -6 dBm input power, our transmitter consumes 23 μA (at 2.2 V) and achieves 10 pJ/bit, which is 42× more efficient than [6], while at a 9 dB lower output power.

TABLE I
PERFORMANCE COMPARISON OF THE PROPOSED TRANSMITTER AND EXISTING IMPLANTABLE TRANSMITTERS

	[5]	[4]	[3]	[6]	This Work
Power Source	Ind.	Ind.	RF	RF	RF
Topology	FRRO	FRLC	FRLC	ILLC	ILRO
Modulation	OOK	FSK	FSK	BPSK	OOK
Uplink (MHz) Downlink (MHz)	4 / 8 70-200	2.64 433	0.125 27.3	450 900	918 306
Current/Power	–	6.75 mW	1 mW	2 mA	.023 mA
Datarate (kbps)	2000	330	80	7000	4000
Min. Supply (V)	1.8	3.55	–	1.5	1.3
P_{out} (dBm,cm)	–	-85,13	-70,10	-24,0	-33,0
Process (um)	1.5	0.5	0.5	0.25	0.13

V. Conclusion

An ultra-low power tag architecture for battery-free continuous streaming biomedical applications has been presented. The incident RF signal simultaneously powers the chip and injection-locks a 3× frequency divider to regenerate an LO frequency for data transmission. The injection-locking process provides a stable LO frequency, high data rate, and >6 meters of data uplink transmission range while consuming 23 μA, the lowest current consumption compared to similar transmitters reported to date.

VI. Acknowledgment

The authors gratefully acknowledge Jagdish Pandey for valuable discussion. This work was partially supported by the National Science Foundation.

References

[1] D. Yeager, F. Zhang, A. Zarrasvand, N. George, T. Daniel, and B. Otis, "A 9 μA, addressable Gen2 sensor tag for biosignal acquisition," *Solid-State Circuits, IEEE Journal of*, vol. 45, pp. 2198 –2209, oct. 2010.

[2] J. Yin, J. Yi, M. Law, Y. Ling, M. C. Lee, K. P. Ng, B. Gao, H. Luong, A. Bermak, M. Chan, W.-H. Ki, C.-Y. Tsui, and M. Yuen, "A system-on-chip EPC Gen-2 passive UHF RFID tag with embedded temperature sensor," *Solid-State Circuits, IEEE Journal of*, vol. 45, pp. 2404 –2420, nov. 2010.

[3] S. Majerus and S. Garverick, "Telemetry platform for deeply implanted biomedical sensors," in *Networked Sensing Systems, 2008. INSS 2008. 5th International Conference on*, pp. 87 –92, june 2008.

[4] R. Harrison, P. Watkins, R. Kier, R. Lovejoy, D. Black, R. Normann, and F. Solzbacher, "A low-power integrated circuit for a wireless 100-electrode neural recording system," in *Solid-State Circuits Conference, 2006. ISSCC 2006. Digest of Technical Papers. IEEE International*, pp. 2258 –2267, feb. 2006.

[5] A. Sodagar, G. Perlin, Y. Yao, K. Najafi, and K. Wise, "An implantable 64-channel wireless microsystem for single-unit neural recording," *Solid-State Circuits, IEEE Journal of*, vol. 44, pp. 2591 –2604, sept. 2009.

[6] F. Kocer and M. Flynn, "A new transponder architecture with on-chip ADC for long-range telemetry applications," *Solid-State Circuits, IEEE Journal of*, vol. 41, pp. 1142 – 1148, may 2006.

[7] Y.-C. Lo, H.-P. Chen, J. Silva-Martinez, and S. Hoyos, "A 1.8V, sub-mW, over 100% locking range, divide-by-3 and 7 complementary-injection-locked 4 Ghz frequency divider," in *Custom Integrated Circuits Conference, 2009. CICC '09. IEEE*, pp. 259 –262, sept. 2009.